Supplementary Information of

Unveiling the structural evolution of oxide surface in liquid water

Xiaoqun Li[1,6], Flavio S. Brigiano[2,3,6], Simone Pezzotti[2,4,6], Xinyi Liu[1,6], Wanlin Chen[2,6], Huiling Chen[1], Ying Li[1], Hui Li[1], Y. Ron Shen[1,5]✉, Marie-Pierre Gaigeot[2]✉, Wei-Tao Liu[1]✉

[1]Physics Department, State Key Laboratory of Surface Physics, Key Laboratory of Micro and Nano Photonic Structures [Ministry of Education (MOE)], Fudan University, Shanghai 200433, China.

[2]Université Paris-Saclay, Univ Evry, CNRS, LAMBE UMR8587, 91025, Evry-Courcouronnes, France,

[3]Current address: Sorbonne Université, Museum National d'Histoire Naturelle, UMR CNRS 7590, IRD, Institut de Minéralogie, de Physique des Matériaux et de Cosmochimie, IMPMC, 75005 Paris, France,

[4]Current address: Physical Chemistry II, Faculty of Chemistry and Biochemistry, Ruhr University Bochum, Universitätsstr. 150, 44780 Bochum, Germany,

[5]Department of Physics, University of California at Berkeley, Berkeley, CA 94702, USA.

[6]These authors contributed equally: Xiaoqun Li, Flavio S. Brigiano, Simone Pezzotti, Xinyi Liu, Wanlin Chen

✉Corresponding author. Email: yrshen@berkeley.edu, mgaigeot@univ-evry.fr, wtliu@fudan.edu.cn

Table of content

S1. Basics of SFG and the nonlinear matrix formalism

S1.1 Basic principle of sum-frequency vibrational spectroscopy

The basic principle of SFG is described elsewhere[1]. Briefly, when the IR frequency (ω_{IR}) is near vibrational resonances, the SF signal (S_{SF}) generated by the incident beams is:

$$S_{SF} \propto \left|\chi_{eff}^{(2)}\right| = |\chi_{NR} + \chi_R|^2 = \left|\chi_{NR} + \sum_q \frac{A_q}{\omega_{IR}-\omega_q+i\Gamma_q}\right|^2, \quad \text{(S1)}$$

where χ_{NR} and χ_R are the non-resonant and resonant contributions, with A_q, ω_q, and Γ_q being the amplitude, frequency, and damping coefficient of the q^{th} resonance mode, respectively. For the SSP (S-SF, S-NIR, P-IR) and PPP (P-SF, P-NIR, P-IR) beam polarization combination, the effective SF amplitudes for an anisotropic interface are[2]:

$$\begin{aligned} A_{SSP} &= \cos\beta_{IR}\, L_{yy}(\omega_{SF})L_{yy}(\omega_{NIR})L_{xx}(\omega_{IR})A_{yyx} \\ &\quad + \sin\beta_{IR}\, L_{yy}(\omega_{SF})L_{yy}(\omega_{NIR})L_{zz}(\omega_{IR})A_{yyz}\,, \\ A_{PPP} &\approx -\cos\beta_{SF}\cos\beta_{NIR}\sin\beta_{IR}\, L_{xx}(\omega_{SF})L_{xx}(\omega_{NIR})L_{zz}(\omega_{IR})A_{xxz} \\ &\quad + \sin\beta_{SF}\sin\beta_{NIR}\sin\beta_{IR}\, L_{zz}(\omega_{SF})L_{zz}(\omega_{NIR})L_{zz}(\omega_{IR})A_{zzz}, \end{aligned}$$

with β_n and $L_{ii}(\omega_n)$ being the beam incident angle and Fresnel coefficients, and {*x, y, z*} referring to the lab coordinates with *z* along the surface normal and *x* in the incident plane.

With inhomogeneous broadening taken into account, the SF output of Equation (S1) becomes[3]:

$$S_{SF} \propto \left|\chi_{NR} + \sum_q \int_{-\infty}^{\infty} \frac{A_q}{\omega_{IR}-\omega'+i\Gamma_q} \frac{1}{\sqrt{2\pi}\sigma_q} \exp\left(-\frac{(\omega'-\omega_q)^2}{2\sigma_q^2}\right) d\omega'\right|^2,$$

where σ_q is the inhomogeneous bandwidth[3]. Figures S1a and S1b show fitting of the experimental spectra taken from the SiO_2-film/water interface at different pH values. The fitting values of Γ_q and σ_q were ~43 and 27 cm^{-1} for the Si-OH band, and ~45 and 28 cm^{-1} for the $Si\text{-}O^-$ band. The resonant amplitudes of the two bands deduced from fitting were plotted versus pH in Figs. S1c and S1d. Dashed and dotted curves in Fig. S1d are theoretical curves calculated from the Gouy-

Chapman-Stern (GCS) model for surface reaction of $SiOH \leftrightarrow SiO^- + H^+$ at ~7 with a single pKa value at ~7[4].

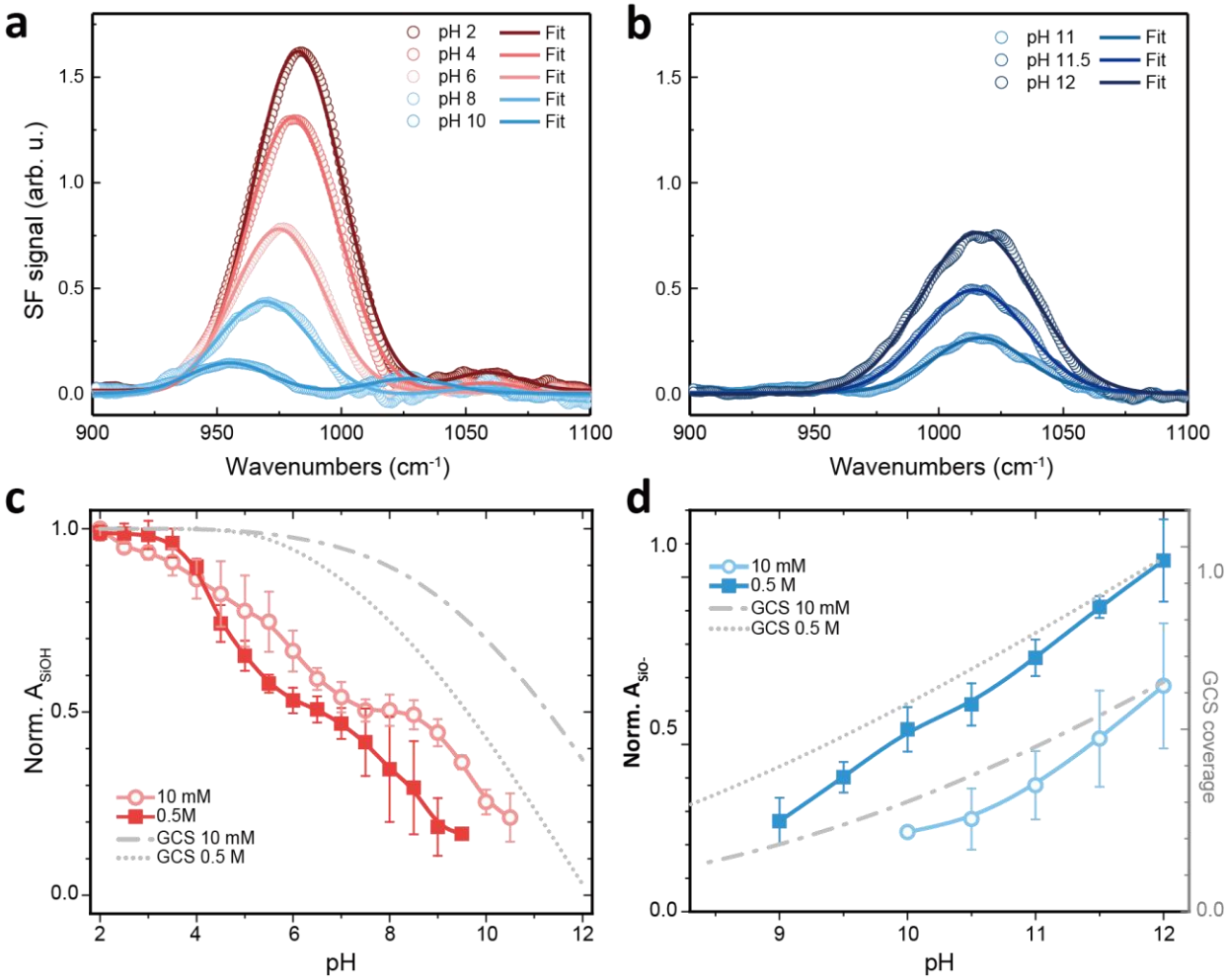

Figure S1 | (**a**) and (**b**) Fits of SF spectra vs. pH. (**c**) and (**d**) Amplitudes of Si-OH and Si-O$^-$ modes deduced for the two ion concentrations, 10 mM (empty symbols) and 0.5 M (filled symbols). The dashed curves are calculated from the single-pKa GCS model of corresponding ion concentrations based on Ref. 5.

S1.2 Nonlinear matrix formalism for local field calculation

The matrix formalism for computing local field strength with nonlinear optical boundary conditions we have developed is described elsewhere[6]. The boundary conditions with the presence of an interfacial polarization sheet $\mathbf{P_s}(\omega)$ are (x parallel to the incident plane, and z along the surface normal):

$$\Delta E_x = \sigma_z = -\frac{4\pi}{\epsilon'} ik_x P_{sz}, \quad \Delta E_y = 0,$$

$$\Delta H_x = \sigma_y = -\frac{4\pi}{c} i\omega P_{sy}, \quad \Delta H_y = \sigma_x = -\frac{4\pi}{c} i\omega P_{sx}.$$

For S-polarized beam (TE wave), we have $\sigma_E = 0, \sigma_H = \sigma_y$; and for P-polarized beam (TM wave), we have $\sigma_E = \sigma_z, \sigma_H = \sigma_x$. In an *n*-layer system, the nonlinear characteristic matrix formalism of the J^{th} interface between j^{th} and $(j+1)^{\text{th}}$ media can then be written as (capital *I, J, N* are indices of interfaces, *i, j, n* are indices of media):

$$\begin{bmatrix} E_{I,1} \\ H_{I,1} \end{bmatrix} = M_2 M_3 \dots M_j \begin{bmatrix} E_{J,j} \\ H_{J,j} \end{bmatrix},$$

$$\begin{bmatrix} E_{J,j} + \sigma_{J,E} \\ H_{J,j} + \sigma_{J,H} \end{bmatrix} = M_{j+1} M_{j+2} \dots M_n \begin{bmatrix} E_{N,n+1} \\ H_{N,\mathrm{n+1}} \end{bmatrix}.$$

M_i is the characteristic matrix of medium with the form of:

$$M_i = \begin{bmatrix} \cos\delta_i & -\frac{i\sin\delta_i}{n_{i,eff}} \\ -in_{i,eff}\sin\delta_i & \cos\delta_i \end{bmatrix},$$

where $n_{i,eff} = n_i \cos\theta_i$ for TE waves, and $n_{i,eff} = n_i / \cos\theta_i$ for TM waves, with n_i being the complex refractive index of, θ_i the beam refraction angle in, and $\delta_i = n_i k_i \cos\theta_i \, d_i$ the wave propagation phase through the i^{th} section of the medium with thickness d_i. Details about the calculation procedure were provided in Ref. 6. The squared products of all local field factors at the Si/SiO_2 and SiO_2/H_2O interfaces, respectively, of a $Si/SiO_2/H_2O$ junction as functions of the SiO_2 film thickness are presented in Fig. 1b of the main text, with reference to the beam geometry in Fig. 1a. The estimated SF intensity in the Si-O stretch range obtained from the maximum local field intensity at the SiO_2/H_2O interface for the case of ~150 nm-thick SiO_2 film in Fig. 1b was about three times of that from an IR-transparent bulk-SiO_2/H_2O interface in the OH stretch range. With SF signals in the latter case being routinely observed, the Si-O stretch signals from the thin-film water interface should be readily detectable.

S2. Properties of Si(5c) species

S2.1 Stability of Si(5c) species versus pH: theoretical calculations

As mentioned in the main text, two kinds of Si(5c) species were formed upon deprotonation of the more acidic SiOH at the amorphous silica surface, i.e., Si(5c)OH^- (66%) and SiO_5^-(33%). We first evaluated the stability of the more abundant Si(5c)OH^- species. We considered a single Si(5c)OH^- on an aqueous 4.5 OH/nm^2 silica surface and simulated its stability in response to changes of pH using DFT-MD metadynamics simulations. The breakage of the Si(5c)OH^- was expected to lead to the formation of two Si(4c), as schematically presented in Figure S2a. In the metadynamic simulations, pH was effectively tuned by changing the protonation states of the two oxygen atoms involved in the formation and breakage of Si(5c)OH^-. Of the two oxygen atoms, the one belonging to the basic (or high-pKa) silanol group hosting the Si(5c)OH^- is labelled O1 (marked in blue in Figure S2a), and the one belonging to the acidic (or low-pKa) silanol group that yielded Si(5c)] is labelled O2 (marked in green, Figure S2a). The first reaction coordinate was chosen as the difference between the coordination number of O2 and O1 with respect to all hydrogen atoms in the system ($C_{OH2-OH1}$), which described the protonation state of the two silanols and the effective pH in the following way: $C_{OH2-OH1}$ = 0 – 1 = -1 if only the acidic silanol (O2) was deprotonated (between pH 4~9); 0 if both silanols were protonated ($C_{OH2-OH1}$ = 1 – 1 = 0) (corresponding to pH < 4) or deprotonated ($C_{OH2-OH1}$ = 0 – 0 = 0) (pK > 9); $C_{OH2-OH1}$=1 – 0 = +1 if only the basic silanol site (O1) was deprotonated. The second reaction coordinate was chosen as the coordination number of O2 with respect to all silicon atoms in the system ($C_{Si\text{-}O\ldots Si}$, green arrow in Figure S2a), to sample the presence or absence of Si(5c)OH^-. This coordinate would take the value of 1.6 when the Si(5c)OH^- species was stable, and a value of 0.9 when Si(5c)OH^- broke into two Si(4c) species. With the above two reaction coordinates, we could hence probe the stability of the molecular species [Si(5c)OH^- or Si(4c)] residing at the surface over different pH ranges.

Figure S2b presents the free energy landscape with different reactive species attached to the respective minima explored by the metadynamics simulation. Minimum 1 was found near $C_{OH2-OH1}$ = -1 and $C_{Si-O...Si}$ = 1.6, corresponding to the case where the low-pKa Si(O2)H was deprotonated, while the high-pKa Si(O1)H group remained protonated and hosted a stable Si(5c); it appeared in the pH range of 4~9. Outside that pH range, when $C_{OH2-OH1} \neq -1$, there was no minimum related to $Si(5c)OH^-$ observed. Instead, minima 2 and 3 were observed for $C_{Si-O...Si} \sim 0.9$, corresponding to the breakdown of $Si(5c)OH^-$ into two Si(4c) when either the high-pKa silanol group is deprotonated (which happens at pH > 9) or both silanols are protonated (pH < 4).

To further confirm the results, we ran two additional *unbiased* DFT-MD simulations on one single deprotonated Si(5c) species [$Si(5c)OH^- \rightarrow Si(5c)O^{--}$, marked by A in Figure S2b] at the aqueous 4.5 OH/nm^2 silica surface. As seen from the absence of a corresponding minimum ($C_{OH2-OH1}$ = 0 and $C_{Si-O...Si}$ = 1.6), the deprotonated Si(5c) systematically breaks into two SiO^- groups after few hundreds of fs, which then remain stable for the entire time duration of the DFT-MD simulations (30 ps). This was due to negative charge increase towards Si(5c) after deprotonation of the already negatively charged $Si(5c)OH^-$ at high pH (average pKa = 7.7) that strongly reducing its electrophilic character, and inducing a cleavage of the O-Si(5c) bond with disappearance of the $Si(5c)OH^-$ species.

Finally, we looked into the stability of the other Si(5c) species, i.e. the SiO_5^-, at high pH (pH > 9). We simulated by *unbiased* DFT-MD the behavior of SiO_5^- at the aqueous 4.5 OH/nm^2 silica surface with all low-pKa and 60 % of the high-pKa silanol groups already deprotonated. The SiO_5^- was found to collapse after few ps of dynamics leading to the formation of one stable SiO^-group.

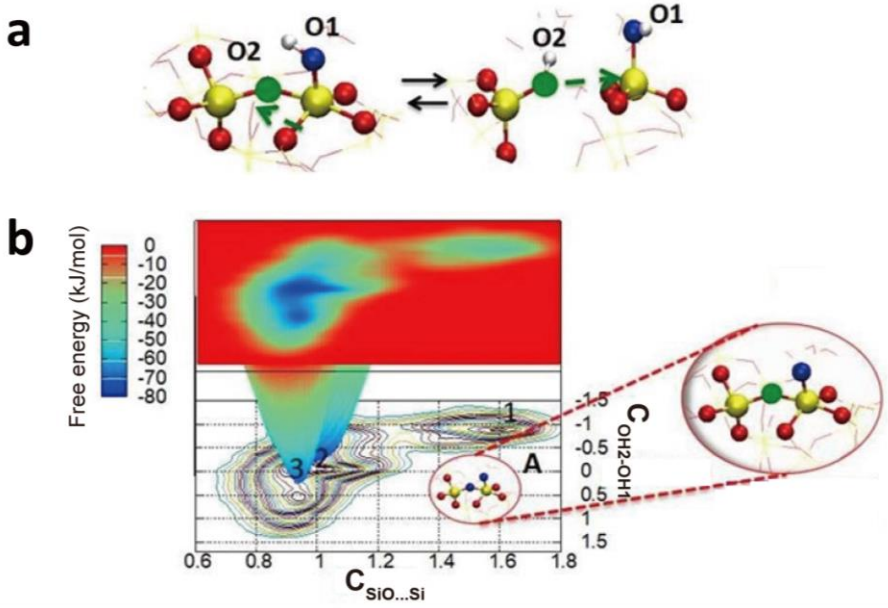

Figure S2 | (a) Scheme of the reaction studied by DFT-MD biased metadynamics simulations. The oxygen atom of the basic (high-pKa) silanol group hosting the Si(5c)OH^- is labelled O1 and marked in blue; the oxygen atom of the acidic (low-pKa) silanol group is labelled O2 (green). A new Si-O bond is created during Si(5c) formation (from right to left), while the same bond has to be cleaved to convert Si(5c) back to two Si(4c) species (from left to right). **(b)** The free energy landscape and associated contour map spanned by $C_{OH2–OH1}$ (horizontal axis) and $C_{Si\text{-}O\ldots Si}$ (vertical axis). Levels in the contour map correspond to increase of 5 kJ/mol. Minimum ① indicates Si(5c)OH^- to be stable at the surface in the pH range 4-9, whereas minima ② and ③ represent two stable Si(4c) species for pH > 9 and pH < 4, respectively. For a reaction with the Si(5c)OH^- further deprotonated to SiO_5^{2-} (marked by capital A), there was no corresponding energy minimum, meaning the product would not be stable.

S2.2 Appearance of Si(5c) species in different models of hydroxylated silica surface

To verify if the results were model-independent, two additional silica surface models with varying degrees of hydroxylation were investigated: 7.6 and 5.5 OH/nm^2 amorphous silica model surfaces[7] in contact with liquid water. We first identified the silanol groups that had the favorable structural properties (in terms of orientations and proximity) for Si(5c) formation based on the results presented in S4 and main text, and then characterized their chemical behavior after deprotonation by unbiased DFT-MD simulations. It was found that once the silanols were deprotonated, the resultant SiO^- indeed approached the neighboring SiO_4 tetrahedron and did the expected nucleophilic attack, leading to the formation of Si(5c). Our results show that when in

contact with water in the pH 4~9 pH range, Si(5c) is systematically and preferentially formed by SiOH groups that satisfy certain orientation and proximity criteria, regardless of the degree of hydroxylation and model adopted to describe the silica surface[7,8].

S3. Theoretical surface coverages and nonlinear optical susceptibilities

S3.1 Theoretical calculation of the surface coverage as a function of pH

We discuss here how we can find the surface coverages of the three surface species: silanols [Si(4c)OH], silanolates (SiO^-), and $Si(5c)^-$ [including $Si(5c)OH^-$ and SiO_5^-], as functions of bulk pH in water. The DFT-MD simulations yielded that ~ 40% (denoted as *a*) of the initial silanol groups were acidic with pKa of 3.9±0.6 (denoted as pK_1) and the rest basic ones with pKa of 7.7±0.9 (denoted as pK_2). We note that the pKa values here were calculated with respect to the surface pH. They will be translated into bulk pH in the later section.

At low and high pH, the three surface species are related to one another through the following reactions

$$\mathrm{SiOH_{(acidic)}} \overset{K_1}{\leftrightarrow} \mathrm{Si(5c)^-} + \mathrm{H^+},$$

$$\mathrm{SiOH_{(basic)}} \overset{K_2}{\leftrightarrow} \mathrm{SiO^-} + \mathrm{H^+},$$

$$\mathrm{Si(5c)^-} \leftrightarrow \mathrm{SiO^-},$$

as illustrated in Figures S3a and S3b, respectively, where H+ is released into the solvent. Based on our DFT-MD results presented in the previous section, we found that breaking of Si(5c)- and the deprotonation of the basic SiOH have the same pH dependence, we therefore can combine the two reactions into one:

$$\mathrm{Si(5c)^-} + \mathrm{SiOH_{(basic)}} \overset{K_2}{\leftrightarrow} 2\mathrm{SiO^-} + \mathrm{H^+}.$$

From the Henderson-Hasselbalch equations, we have the following relations between surface coverage of SiOH, $Si(5c)^-$ and SiO^- (C_{SiOH}, $C_{Si(5c)^-}$, and C_{SiO^-}, with 1 referring to a full coverage of SiOH not being deprotonated) and the surface pH (pH_S):

$$pH_S = pK_1 + \log_{10}\left(\frac{C_{Si(5c)^-}}{C_{SiOH_{acidic}}}\right),$$

$$pH_S = pK_2 + \log_{10}\left(\frac{(C_{SiO^-})^2}{C_{SiOH_{basic}}\, C_{Si(5c)^-}}\right).$$

from which we find:

$$C_{Si(5c)^-}(pH_S) = C_{Si(5c)^-}^{produced} - C_{Si(5c)^-}^{consumed} = a\frac{10^{pH_S-pK_1}}{1+10^{pH_S-pK_1}}\left(1-\frac{10^{pH_S-pK_2}}{1+10^{pH_S-pK_2}}\right), \quad \text{(S2)}$$

$$C_{SiO^-}(pH_S) = (1-a)\frac{10^{pH_S-pK_2}}{1+10^{pH_S-pK_2}} + a\frac{10^{2pH_S-pK_1-pK_2}}{(1+10^{pH_S-pK_1})(1+10^{pH_S-pK_2})}, \quad \text{(S3)}$$

$$C_{SiOH}(pH_S) = 1 - C_{SiO^-}(pH_S) - C_{Si(5c)^-}(pH_S). \quad \text{(S4)}$$

where a is the percentage of the initial acidic silanol groups (40% of silanols).

Because of inhomogeneity of the surface structure, the values of pK_1 and pK_2 (with respect to the surface pH) in our DFT-MD simulations appear as distributions that can be approximated by Gaussian functions centered at 3.9 and 7.7, respectively, with corresponding standard deviations of 0.6 for pK_1 and 0.9 for pK_2.

The surface pH (pH_S) and bulk pH, or the surface and bulk H+ concentrations, $n_S\left(H^+\right)$ and $n_B\left(H^+\right)$, are related by the surface potential ϕ created by the surface charge density σ given by $\sigma(pH) = (C_{Si(5c)^-} + C_{SiO^-})\,\rho_{SiOH}\,e$, where ρ_{SiOH} is the surface density of SiOH for a neutral interface at low pH and e is the unit electrical charge. From the modified Poisson-Boltzmann equation[9,10], we have:

$$n_B(H^+) = \frac{n_{Surface}(H^+)\left(1+2\upsilon\, sinh^2\left(\frac{e\phi}{2k_BT}\right)\right)}{\exp(-\frac{e\phi}{k_BT})},$$

$$\phi_0 = \phi(z=0) = -\frac{2k_BT}{e}\sinh^{-1}\left\{\sqrt{\frac{1}{2\upsilon}\left[\exp\left(\frac{\sigma^2\upsilon}{4n_0\varepsilon\varepsilon_0k_BT}\right)-1\right]}\right\}, \quad \text{(S5)}$$

where ϕ is the electric potential in function of the distance in z-direction from the surface, σ, n_0, k_B, T, e, ε, and ε_0 are the surface charge density, the ion concentration in the bulk, the Boltzmann constant, the temperature in Kelvin, the elementary charge, the relative dielectric constant of liquid water and the dielectric constant of vacuum. The parameter υ is expressed as $\upsilon = 2a^3n_0$, where

we adopt a = 0.7 nm as the Bjerrum length to account for the ion size in water at room temperature[11,12].

The calculated surface pH_S and bulk pH for our case of two different ion concentrations, 10 mM and 0.5 M (see experimental conditions), are plotted in Fig. S3c. Accordingly, the values of pK_1 and pK_2 with respect to bulk pH are changed to 6.7 ± 0.6 and 11.6 ± 0.9 at 10 mM ion concentration, and $pK_1 = 4.7 \pm 0.6$ and $pK_2 = 9.8 \pm 0.9$ at 0.5 M ion concentration, as denoted by the dotted lines in Fig. S3c. From Equation (S5), we can thus translate the theoretical pKa values (calculated with respect to surface pH) to bulk pH units, as illustrated in Figure S3c. Taking these bulk pKa values and adopting the same method discussed in the previous section, we can then convert pH_S and find the coverages of different species as functions of bulk pH, as presented in Fig. 4a of the main text for the case of 10 mM ion concentration.

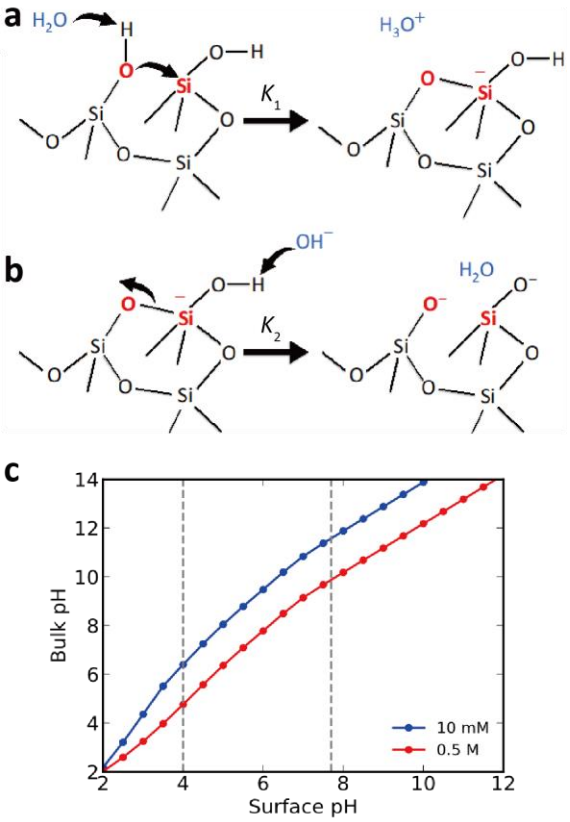

Figure S3 | (a) Formation of $Si(5c)^-$ species. **(b)** Breaking of $Si(5c)^-$ species. **(c)** Calculated bulk pH versus surface pH values.

S3.2 Theoretical calculation of SFG spectra as a function of pH

The DFT-MD SFG spectrum of the silica/water interface in the Si-O stretching region was calculated from $\left|\chi^{(2)}_{total}(\omega, pH)\right|^2$, with $\chi^{(2)}_{total}(\omega, pH)$ being the total SFG surface nonlinear susceptibility given by

$$\chi^{(2)}_{total}(\omega, pH) = \sum_j \; C_j(pH)\, \bar{\chi}^{(2)}_j(\omega),$$

where $\bar{\chi}^{(2)}_j(\omega)$ is the surface nonlinear susceptibility of the j^{th} surface species at full coverage including Si-OH, Si(5c)-OH$^-$, and Si-O$^-$, and $C_j(pH)$ is the fractional surface coverage of the j^{th} surface species at a given (bulk) pH (see Sec. S3.1). To calculate $\bar{\chi}^{(2)}_{j,xxz}(\omega)$ (experimentally probed by SFG with SSP polarization combination), we adopted the same methodology previously developed for surface $\chi^{(2)}(\omega)$ spectra of both water and SiO-H in the O-H stretch range[13], which had shown excellent agreement with experiments[14-17]. We used the following expression in the calculation:

$$\bar{\chi}^{(2)}_{j,xxz}(\omega) = \frac{i}{k_B T \omega} \int_0^\infty dt\, \mathrm{e}^{-\mathrm{i}\omega t} \left\langle \dot{\alpha}_{j,xx}(t) \dot{\mu}_{j,z}(0) \right\rangle,$$

where $\mu_z(0)$ and $\alpha_{xx}(t)$ refer to the z and xx components of the dipole and polarizability of the surface-group in the laboratory frame, and the angular brackets denote an average of the product. The calculated $|\bar{\chi}^{(2)}_{j,xxz}(\omega)|$ spectra for the three surface species, Si-OH, Si(5c)-OH$^-$, and Si-O$^-$, are shown in Extended Data Fig. 4; they peaked at ~840, 920, and 1000 cm^{-1}, respectively, and their profiles hardly change with pH. The total surface nonlinear susceptibility is given by:

$$\chi^{(2)}_{ssp}(\omega, pH) = \left(C_{SiOH}(pH) - \; C_{Si(5c)^-}(pH)\right) \; \bar{\chi}^{(2)}_{SiOH}(\omega) + \; C_{Si(5c)^-}(pH) \; \bar{\chi}^{(2)}_{Si(5c)^-}(\omega)$$
$$+ C_{SiO^-}(pH)\, \bar{\chi}^{(2)}_{SiO^-}(\omega),$$

from which the $|\chi^{(2)}_{ssp}(\omega, pH)|^2$ spectra can be found as presented in Figs. 4b and 4c of the main text in comparison with the experimentally observed spectra.

S3.3 Consistency between the discovery of Si(5c)- species & SHG titration experiments

According to Ref. 10 the effective surface nonlinear susceptibility for the reflected second harmonic generation (SHG) at 2ω has the expression

$$\chi_{eff}^{(2)}(2\omega) = \chi_{BIL}^{(2)} + \chi_{DL}^{(2)}, \quad \text{(S6)}$$

$$\chi_{DL}^{(2)} = \chi_{Bulk}^{(3)} \Psi, \quad \text{(S7)}$$

$$\Psi = \int_0^\infty E_0(z') e^{i\Delta k_z z'} dz', \quad \text{(S8)}$$

where Δk_z is the phase mismatch of the reflected SHG, $\chi_{BIL}^{(2)}$ is the second-order nonlinear susceptibility of the BIL (bonded interfacial layer) water[18], Ψ is the phase-modulated potential difference across the diffuse layer (DL), and $\chi_{Bulk}^{(3)}$ is the third-order nonlinear susceptibility of bulk water. It was found that $\chi_{Bulk}^{(3)}$ = (9.56 ± 1.87) × 10^{-22} m^2/V^2 at 2ω ~ 20,000 cm^{-1}[12]. Since we knew the surface charge density σ from the fractional surface coverages of Si(5c) and SiO^- and the surface potential $\phi(z)$ from the solution of the modified Debye-Boltzmann equation as functions of (bulk) pH (See Sec. S3.1), we could obtain the field $E_0(z')$ from $E_0(z')\hat{z} = -\nabla\phi(z)$, and then deduce the complex Ψ from Equation (S8) with Δk_z^{-1}= 25 nm[18]. We thus can calculate the $\chi_{DL}^{(2)}$ as a function of pH from Equation (S7).

As the change in $\chi_{BIL}^{(2)}$ with pH was shown in previous studies to be much smaller than the change in the $\chi_{DL}^{(2)}$ term[17], we hence simply took the $\chi_{eff}^{(2)}$ value at pH 2 (corresponding to σ = 0) from the SHG results reported in Ref. 19 as $\chi_{BIL}^{(2)}$ for all calculations. We then obtained the total $\chi_{SHG}^{(2)}$ from the sum of $\chi_{BIL}^{(2)}$ and $\chi_{DL}^{(2)}$, as plotted $|\chi_{SHG}^{(2)}|$ versus pH in Fig. 4e (main text) in comparison with the experimental results reported in Ref. 19.

S4. Structure characterization of local environments for Si(5c) formation

Here we focus on specific local structures of the interface that could lead to the formation of Si(5c) species. We first considered the possible role of water in Si(5c) formation using the model surface that had a surface SiOH density of 4.5/nm^2. We studied if the silanol acidity and Si(5c) formation could be influenced by the silanols exposure to water. Figure S4a describes the heterogeneous distribution of water density in the bonded interfacial layer (BIL) with silanol groups (circles with index number) at different places. Red circles and indices refer to silanols that would deprotonate to form Si(5c), and the black indices to silanols that would deprotonate to form Si-O$^-$. As shown in the Table of Fig. S4b, we found *no correlation* between Si(5c) formation and how SiOH initially interacts with neighboring water.

We next considered the possibility that Si(5c) could result from deprotonation of special types of silanols (e.g. vicinal vs isolated) or SiOH having specific H-bonding with adjacent water molecules (i.e. SiOH bonded to water molecules with a donor bond, an acceptor bond, both donor and acceptor bonds, or no bond at all.) Again, as summarized in the table of Fig. S4b, we found no correlation between Si(5c) formation and H-bonding of SiOH. We can therefore conclude that despite water is an essential reactant in silanol deprotonation, its influence on the acidity of SiOH and Si(5c) formation is not significant.

We then questioned whether there were specific surface morphological factors that can affect the Si(5c) formation. Plotted in Fig. S5a are the Si radial distributions around the oxygen atom of each of the eight SiOH groups on the 4.5 OH/nm^2 silica surface, taking into accounts all Si atoms in the system. In each radial distribution curve, the first peak (at r > 2.5 Å) corresponds to the distance between the oxygen atom and its closest neighboring Si atom that is *not* covalently bonded to it. The three distributions plotted in red, blue, and black dashed curves are the only ones in which the first peak appears for $r_{O\text{-}Si}$ < 3.5 Å. Interestingly, they were the only three SiOH groups

that formed Si(5c) upon deprotonation. This suggests that the close proximity between the oxygen atom of a given SiOH and a neighboring Si atom is important for the Si(5c) formation.

We also question the effect of SiOH orientation towards a neighboring SiO_4 on Si(5c) formation. We plot in Fig. S5b the probability of Si(5c) formation as a function of the angle *x* (defined as the angle between the two blue arrows in the sketch at the top of Fig. S5b) that describes the relative orientation of the silanol Si-OH bond (that performs the nucleophilic attack) with respect to the SiO_4 tetrahedron being attacked, and the distance between the oxygen atoms, i.e. O* of SiOH and O of SiO_4 labelled in Fig. S5b. Three peaks appear in this plot, all are obtained for *x* ~ 90^o, and each of the peaks is obtained for a different value of the O*-O distance. They reflect ideal geometries for the formation of a Si(5c) species that best avoid steric hindrance between the three oxygens of SiO_4 and the SiOH during the nucleophilic attack. The above structural analysis shows that proximity and appropriate relative orientation between SiOH and a neighboring SiO_4 tetrahedron are key factors for the formation of Si(5c).

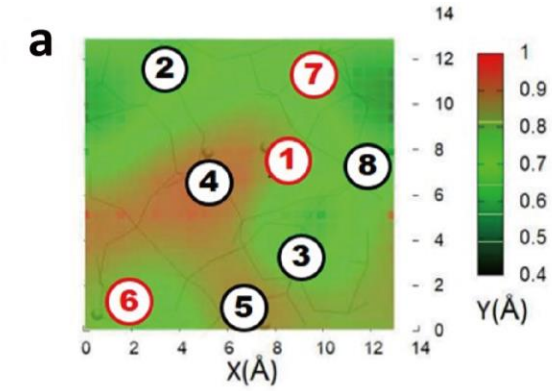

b

Index	Type	HBond	pKa	Conjugated base
①	Vicinal	D		Si(5c)
②	Vicinal	D	7.8	SiO-
③	Isolated	A/D	8.2	SiO-
④	Isolated	A/D	6.0	SiO-
⑤	Vicinal	D	8.2	SiO-
⑥	Isolated	A/D	4.5	Si(5c)
⑦	Vicinal	A/D	3.3	Si(5c)
⑧	Vicinal	A/D	8.3	SiO-

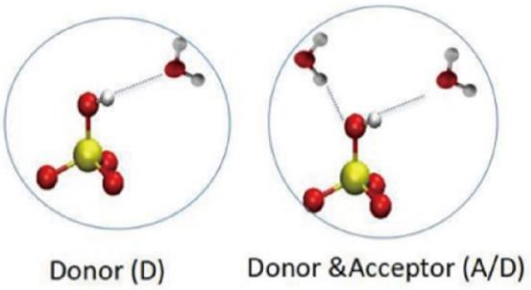

Figure S4 | (a) Water density map in the bonded interfacial layer above the 4.5 SiOH/nm^2 silica surface. The color coding (vertical scale in the plots) goes from black (low density of water) to red (high density of water). The eight surface Si-OH silanols at the model silica surface are labelled by their index numbers (in circles); the silanols that transform into Si(5c) species, once deprotonated, are labelled in red and the others in black. **(b),** Table describing some properties of each indexed silanol, i.e., isolated or vicinal, H-bonding pattern with water molecules in the BIL, pKa value and the nature of the conjugate base [SiO^- or Si(5c)]. We note that silanols that are not H-bonded to water are not statistically relevant at the investigated interface. On the right of **(b)** is the scheme of the relevant H-bonding patterns obtained in our DFT-MD simulations.

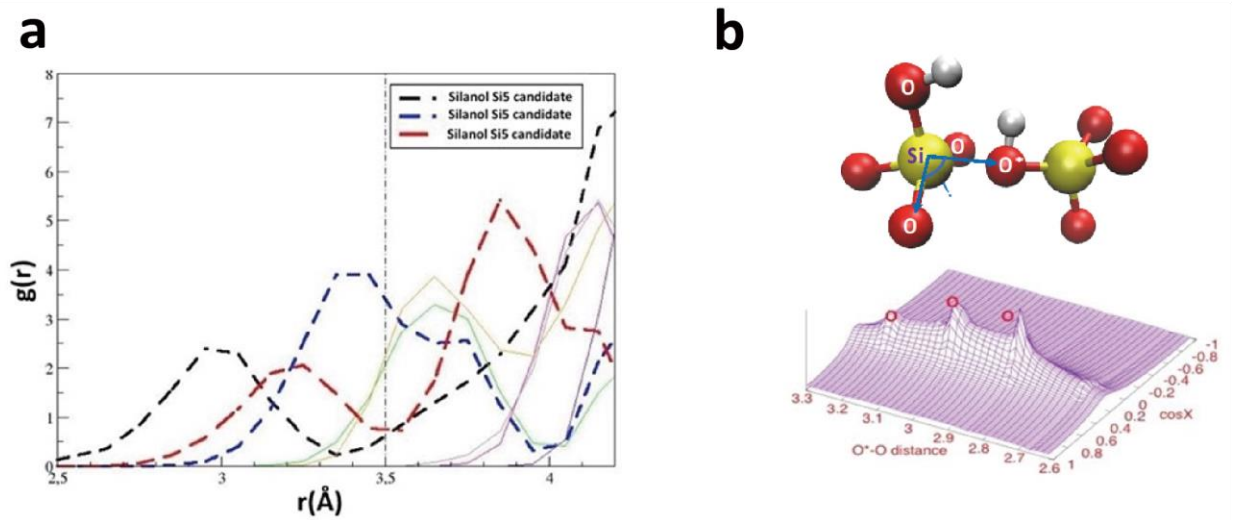

Figure S5 | (a) Si-O radial distribution curves of non-covalently bonded Si atoms around the oxygen atom of each of the eight SiOH groups located on the surface of the 4.5 OH/nm^2 silica model. There are 8 plots reported, among which the red, black and blue dashed ones correspond to the SiOH groups whose deprotonation leads to the formation of Si(5c). **(b)** The top frame is a snapshot from the DFT-MD simulations that describes the SiO_4 tetrahedron in optimum orientation with respect to the reactive SiOH for the formation of the Si(5c) species. The bottom frame shows the distribution of Si(5c) formation with as a function of the O*-O distance and of the angle x (both are defined in the top frame) between SiOH and SiO_4. The three peaks marked with red circles identify the three most probable geometries for Si(5c) formation found in our simulations.

References:

1. Wang, H. et al. Gate-Controlled Sum-Frequency Vibrational Spectroscopy for Probing Charged Oxide/Water Interfaces. *J. Phys. Chem. Lett* **10**, 5943-5948 (2019).
2. Liu, W. & Shen, Y. R. Surface Vibrational Modes of Alpha-Quartz(0001) Probed by Sum-Frequency Spectroscopy. *Phys. Rev. Lett.* **101** (2008).
3. Ostroverkhov, V., Waychunas, G. A. & Shen, Y. R. Vibrational Spectra of Water at Water/Alpha-Quartz (0001) Interface. *Chem. Phys. Lett.* **386**, 144-148 (2004).
4. Behrens, S. H. & Grier, D. G. The Charge of Glass and Silica Surfaces. *The Journal of Chemical Physics* **115**, 6716-6721 (2001).
5. Farnan, I. & Stebbins, J. F. The Nature of the Glass Transition in a Silica-Rich Oxide Melt. *Science* **265**, 1206-1209 (1994).
6. Shi, H., Zhang, Y., Wang, H. & Liu, W. Matrix Formalism for Radiating Polarization Sheets in Multilayer Structures of Arbitrary Composition. *Chin Opt Lett* **15** (2017).
7. Masini, P. & Bernasconi, M. Ab Initio Simulations of Hydroxylation and Dehydroxylation Reactions at Surfaces: Amorphous Silica and Brucite. *Journal of Physics: Condensed Matter* **14**, 4133 (2002).
8. Ugliengo, P. et al. Realistic Models of Hydroxylated Amorphous Silica Surfaces and MCM-41 Mesoporous Material Simulated by Large-Scale Periodic B3LYP Calculations. *Adv. Mater.* **20**, 4579-4583 (2008).
9. Urashima, S., Myalitsin, A., Nihonyanagi, S. & Tahara, T. The Topmost Water Structure at a Charged Silica/Aqueous Interface Revealed by Heterodyne-Detected Vibrational Sum Frequency Generation Spectroscopy. *J. Phys. Chem. Lett* **9**, 4109-4114 (2018).
10. Dalstein, L., Chiang, K. & Wen, Y. Direct Quantification of Water Surface Charge by Phase-Sensitive Second Harmonic Spectroscopy. *The Journal of Physical Chemistry Letters* **10**, 5200-5205 (2019).
11. Andelman, D., Orland, H. & Borukhov, I. Steric Effects in Electrolytes: A Modified Poisson-Boltzmann Equation. *Phys. Rev. Lett.* **79**, 435-438 (1997).
12. Bazant, M. Z., Ajdari, A. & Kilic, M. S. Steric Effects in the Dynamics of Electrolytes at Large Applied Voltages. II. Modified Poisson-Nernst-Planck Equations. *Phys. Rev. E* **75**, 21503 (2007).
13. Khatib, R. et al. Molecular Dynamics Simulations of SFG Librational Modes Spectra of Water at the Water-Air Interface. *The Journal of Physical Chemistry C* **120**, 18665-18673 (2016).
14. Tuladhar, A. et al. Ions Tune Interfacial Water Structure and Modulate Hydrophobic Interactions at Silica Surfaces. *J. Am. Chem. Soc.* **142**, 6991-7000 (2020).
15. Pezzotti, S., Galimberti, D. R., Shen, Y. R. & Gaigeot, M. Structural Definition of the BIL and DL: A New Universal Methodology to Rationalize Non-Linear $\chi^{(2)}(\Omega)$ SFG Signals at Charged Interfaces, Including $\chi^{(3)}(\Omega)$ Contributions. *Phys. Chem. Chem. Phys.* **20**, 5190-5199 (2018).
16. Pezzotti, S., Galimberti, D. R. & Gaigeot, M. Deconvolution of BIL-SFG and DL-SFG Spectroscopic Signals Reveals Order/Disorder of Water at the Elusive Aqueous Silica Interface. *Phys. Chem. Chem. Phys.* **21**, 22188-22202 (2019).
17. Pezzotti, S., Galimberti, D. R. & Gaigeot, M. 2D H-Bond Network as the Topmost Skin to the Air-Water Interface. *The Journal of Physical Chemistry Letters* **8**, 3133-3141 (2017).
18. Wang, H., Hu, X. & Wang, H. Charge-Induced $\chi^{(3)}$ Susceptibility in Interfacial Nonlinear Optical Spectroscopy Beyond the Bulk Aqueous Contributions: The Case for Silica/Water Interface. *The Journal of Physical Chemistry C* **125**, 26208-26215 (2021).
19. Ong, S., Zhao, X. & Eisenthal, K. B. Polarization of Water Molecules at a Charged Interface:

Second Harmonic Studies of the Silica/Water Interface. *Chem. Phys. Lett.* **191**, 327-335 (1992).